

# Templated assembly of metal nanoparticles in nanoimprinted patterns for metal nanowire fabrication

Eun-Uk Kim<sup>1</sup>, Kang-Jun Baeg<sup>1,2</sup>, Yong-Young Noh<sup>3</sup>,  
Dong-Yu Kim<sup>1,2</sup>, Takhee Lee<sup>1</sup>, Inkyu Park<sup>4,5</sup> and  
Gun-Young Jung<sup>1,5</sup>

<sup>1</sup> Department of Materials Science and Engineering and Program for Integrated System (PIMS), Gwangju Institute of Science and Technology, Gwangju 500-712, Korea

<sup>2</sup> Heeger Center for Advanced Materials, Gwangju Institute of Science and Technology, Korea

<sup>3</sup> Convergence Components and Materials Laboratory, Electronics and Telecommunications Research Institute, Daejeon 305-350, Korea

<sup>4</sup> Department of Mechanical Engineering, Korea Advanced Institute of Science and Technology, Daejeon 305-701, Korea

E-mail: [inkyu.park@kaist.ac.kr](mailto:inkyu.park@kaist.ac.kr) and [gyjung@gist.ac.kr](mailto:gyjung@gist.ac.kr)

Received 16 June 2009, in final form 20 July 2009

Published 11 August 2009

Online at [stacks.iop.org/Nano/20/355302](http://stacks.iop.org/Nano/20/355302)

## Abstract

We have developed a new method that combines nanoimprint lithography and metal nanoparticle solution processing for fabricating metal nanowires. A polymer template with nanoscale features, fabricated by nanoimprint lithography, provided physical reservoirs which were filled with a silver nanoparticle solution during the spin-coating. After the lift-off process, the defined silver nanoparticle patterns were annealed to enhance the conductivity for use as electrodes. Silver nanowire patterns (500 nm linewidth with a 300 nm gap) were fabricated without using an expensive high-vacuum system for metal deposition. This method demonstrated pattern resolution enhancement compared with ink-jet printing which inherently suffers from ink spreading on the substrate surface. By using this method, organic thin film transistors composed of the solution-processed silver source/drain electrodes with a channel length of 300 nm were fabricated and showed comparable behaviors to those with vacuum-deposited electrodes.

## 1. Introduction

The use of metal nanoparticle solutions has attracted considerable attention for fabricating metallic wires at the micro- or nanoscale, particularly as an alternative to physical deposition methods such as sputtering and evaporation techniques [1–6]. Compared to conventional patterning methods based on photolithography, printing methods that use metal nanoparticle solutions, such as ink-jet printing [1, 2], screen printing [3, 4] and microcontact printing [5], use less organic solvent and toxic materials due to their direct patterning nature. Therefore, they are more environmentally friendly than the conventional microfabrication methods and

they can lessen the manufacturing cost by avoiding the use of expensive vacuum systems.

Printing processes have been widely investigated with various kinds of inks, such as metal nanoparticles, conductive polymers, organic semiconductors and electromechanical and bioactive materials, depending on the purpose of the experiment [6]. However, it is difficult to produce patterns with a fine resolution due to the inherent nature of ink solutions which results in diffusion or spreading on the substrate surface such that only micrometer-scale patterning has been demonstrated with these printing techniques.

To overcome this challenge, an alternative method is proposed for fabricating nanoscale metal patterns by a solution deposition process combined with a nanoimprint lithography technique. Nanoimprint lithography is an

<sup>5</sup> Authors to whom any correspondence should be addressed.

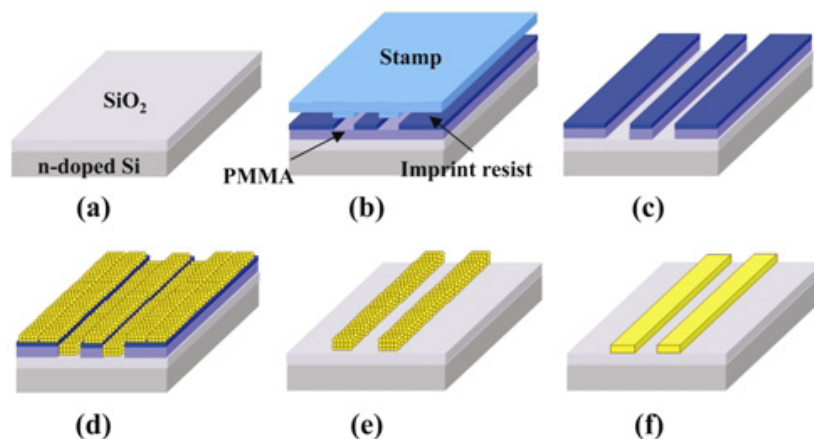


**Figure 1.** The metal nanowire fabrication process combining nanoimprint lithography and nanoparticle solution processing: (a) a clean SiO<sub>2</sub> substrate; (b) nanoimprinting of the resist layer; (c) pattern transfer to the PMMA layer by reactive ion etching (RIE); (d) spin-coating of the metal nanoparticle solution; (e) PMMA layer lift-off; (f) annealing of metal nanoparticle patterns for conversion into conductive metallic structures.

(This figure is in colour only in the electronic version)

emerging methodology with the potential to overcome the limit of pattern resolution in the conventional optical lithographic process, therefore in 2003 it was included in the International Technology Roadmap for Semiconductors (ITRS) as a prominent tool for patterning sub-32 nm nodes [7–9]. Park *et al* fabricated nanoscale gold patterns from a gold nanoparticle solution by a direct nanoimprinting method, where the gold nanoparticle solution was dispensed on the substrate and then imprinted directly using a poly-(dimethylsiloxane) (PDMS) stamp with the corresponding nanoscale features [10, 11]. However, this method has limitations such as: (1) a residual layer of metal nanoparticles at occasional areas, which may need wet metal etchants for removal and can therefore roughen the surface and alter the feature size of the fabricated metallic patterns; (2) high dependency of the cross-sectional profile of the metal nanoparticle pattern on the stamp trench width due to the different balance of gravitational and capillary forces within the stamp trenches during filling with the the gold nanoparticle solution [10].

To resolve these problems, in this research, a polymer template with nanoscale trenches was first prepared by a nanoimprint lithography technique and then the metal nanoparticle solution was spin-coated on it. The polymer trenches provide physical reservoirs to confine the metal nanoparticle solution ink during the following spin-coating, thereby preventing the ink from spreading, which is common in the ink-jet printing technique, and enabling nanoscale patterns from the metal ink solution as a result. After polymer template lift-off, the remaining metal nanoparticle patterns are annealed to enhance the conductivity along the nanoparticle wires, which is a prerequisite for their use as electrodes. The advantage of this process is that it does not require any expensive high-vacuum metal evaporation systems, which require an idling time in order to reach high vacuum. Additionally, if equipped with rolling-based imprinting and a doctor blade system to dispense the metal nanoparticle

solution, this technique enables a continuous process from initial substrate loading to final metallic patterns.

## 2. Experimental details

### 2.1. Nanoimprint lithography

The overall process scheme for generation of metallic patterns using a metal nanoparticle solution is illustrated in figure 1. Nanoimprint lithography was performed on a heavily doped silicon substrate ( $n^{++}$ , resistance 1–5  $\Omega \text{ cm}^{-1}$ ) with a thermally grown silicon dioxide layer (of thickness 50 nm). Prior to the nanoimprinting process, the substrate was treated with a 1:1 mixture of hydrochloric acid and hydrogen peroxide followed by cleaning with acetone, iso-propylalcohol (IPA) and deionized (DI) water in an ultrasonic bath for 10 min each to remove any contaminants. Poly(methyl methacrylate) (PMMA, Aldrich, average  $M_w \sim 996\,000$ ) dissolved in chlorobenzene (4 wt% PMMA concentration) was used as the pattern transfer layer. The PMMA solution was spun at 4000 rpm for 40 s on the substrate and baked at 120 °C for 3 min on a hotplate to obtain a 200 nm thick film. For the UV-nanoimprint process, we formulated a low viscosity UV-curable nanoimprint resist solution that consisted of a UV-curable PDMS material (DMS-R05, Gelest, 87 wt%), a cross-linker (ethylene glycol dimethacrylate, Aldrich, 10 wt%) and a radical initiator (Irgacure 184, Ciba, 3 wt%) [12].

Prior to the nanoimprinting process, the stamp surface was coated with a self-assembled monolayer of tridecafluoro-1,1,2,2-tetrahydrooctyltrichlorosilane in the vapor phase for easy stamp detachment from the imprinted resist by reducing the surface energy of the stamp [13]. Then, the formulated UV-nanoimprint resist material was spin-coated on top of the PMMA layer at 6000 rpm for 150 s. UV light cured the resist that was sandwiched between the stamp and the substrate while being subjected to an imprinting pressure of 5 bar using a nanoimprint machine (NANOSIS 620, Nano & Device) as shown in figure 1(b). After the nanoimprinting process, the

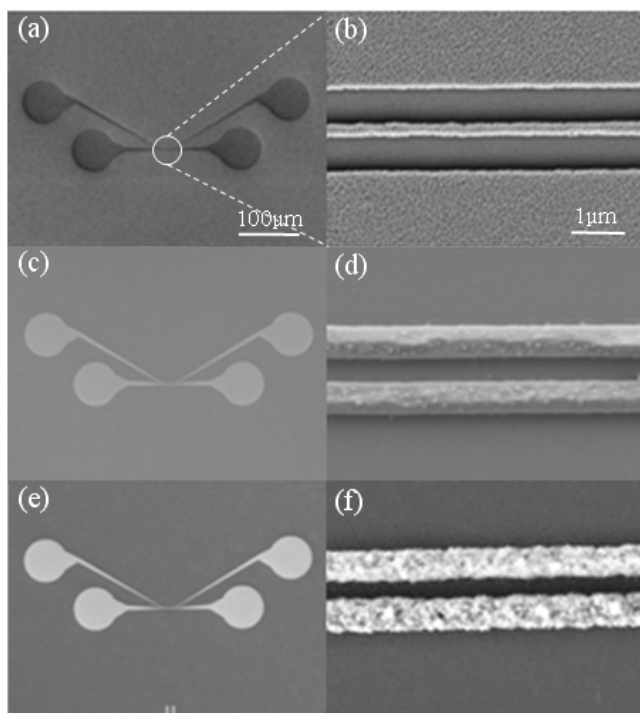


**Figure 2.** FE-SEM images of the fabricated nanostructures: (a), (b) a polymer template after pattern transfer to the under-layer; (c), (d) a silver nanoparticle pattern after the lift-off process; (e), (f) their corresponding silver metallic pattern after annealing at 120 °C for 8 h.

printed pattern was treated in a  $\text{CF}_4$  gas plasma at 20 W and 20 mTorr for 20 s to remove any residual resist layer under the imprinted trenches. Then, oxygen plasma treatment was carried out at 20 W and 20 mTorr for 150 s to transfer the pattern to the PMMA layer. Because the cured resist layer has a high resistance to oxygen plasma etching, the imprinted pattern was successfully transferred to the pattern transfer layer without damaging the imprinted patterns as depicted in figure 1(c). Figure 2(b) shows a field emission scanning electron microscope (FE-SEM) image of two 500 nm wide line patterns with a 300 nm gap after the pattern transfer; these are connected to electric pads at both ends through a fan-out structure as shown in figure 2(a). The grooves in the polymer template act as reservoirs for the silver nanoparticle solution in the following spin-coating process.

### 2.2. Coating of silver nanoparticle solution

A silver nanoparticle (Ag NP) solution from Harima Chemicals Inc. was used for the solution process. The original Ag NP solution is dispersed in tetradecane at a concentration of 60 wt% for the purpose of ink-jet printing. Since the Ag NP solution as-received was too viscous for uniform coating by a spin-coating method, it was diluted with heptane down to 20 wt% concentration. The particle size was 3–7 nm with a mean diameter of 5 nm. The Ag NP solution (50  $\mu\text{l}$ ) was dropped on the imprinted polymer template (1.5  $\times$  1.5  $\text{cm}^2$ ) and spin-coated at 2000 rpm for 30 s. The coated sample was baked on a hotplate at 100 °C for 2 min to evaporate the heptane

solvent and the polymer template (imprinted resist/PMMA bilayer) was then removed by soaking in acetone with delicate hand stirring, resulting in inversely replicated Ag NP patterns, as shown in figures 2(c) and (d). The defined Ag NP patterns were annealed to improve the conductivity in a vacuum oven.

### 2.3. Fabrication of poly(3-hexylthiophene) (P3HT) organic field effect transistors (OFETs)

The OFETs had a bottom-gate/bottom-contact configuration, where the channel length ( $L = 300$  nm) was defined by the distance between the two parallel silver nanowires fabricated on top of a 50 nm thick  $\text{SiO}_2/\text{Si}(\text{n}^{++})$  wafer. After fabricating the source–drain (S/D) electrodes, the samples were cleaned with acetone, IPA and dried by a flow of nitrogen gas. Subsequently, the sample with the S/D electrodes was covered with hexamethyldisilazane (HMDS) in a vacuum desiccator for 10 h. P3HT solution (10 mg  $\text{ml}^{-1}$  in 1,2,4-trichlorobenzene, TCB) was spin-coated onto the HMDS-treated samples in a  $\text{N}_2$ -purged glovebox and baked at 150 °C for 30 min to remove the residual TCB solvent.

## 3. Results and discussion

The initial Ag NP nanowires were insulating because each nanoparticle was coated with organic dispersant. Therefore, an annealing process should be performed not only for removal of the dispersant surrounding the NPs, but also for sintering the individual Ag NPs to generate a continuous electrical path for use as a metallic application. As nanoparticles are generally unstable due to their high surface area to volume ratio, the atoms on the nanoparticle surface have a higher surface energy. This is why melting occurs at a much lower temperature for nanoparticles than for the bulk state [14]. The optimum annealing temperature and time must be determined to guarantee an electrical conductivity close to that of the bulk silver film.

Ag NP bulk films 250 nm thick were prepared on a silicon oxide substrate by spin-coating at 2000 rpm for 30 s, followed by thermal treatment in a vacuum oven at 100, 120 and 140 °C. Electrical resistivity was measured with time at each temperature by the four-point probe method, from which electrical conductivity was calculated and plotted in figure 3(a). The conductivity of a 30 nm thick silver film deposited by electron-beam evaporation was referenced for comparison. The electrical conductivity increased with the sintering time and became saturated in the range of  $10^6$ – $10^7$   $\text{S m}^{-1}$ , which was lower (within one order of magnitude) than that of the evaporated silver film,  $6.2 \times 10^7$   $\text{S m}^{-1}$ . On increasing the annealing temperature, the ramping time to the saturated value of conductivity decreased exponentially, i.e. more than 20 h at 100 °C, 8 h at 120 °C and 2 h at 140 °C.

Based on these results, the annealing process was performed directly with the fabricated 500 nm wide Ag NP line patterns. The morphology of the annealed silver nanowire was greatly affected by the annealing temperature. As shown in figures 3(b)–(d), critical changes were observed in the morphology of the metal nanowires annealed at 140 °C for 2 h,

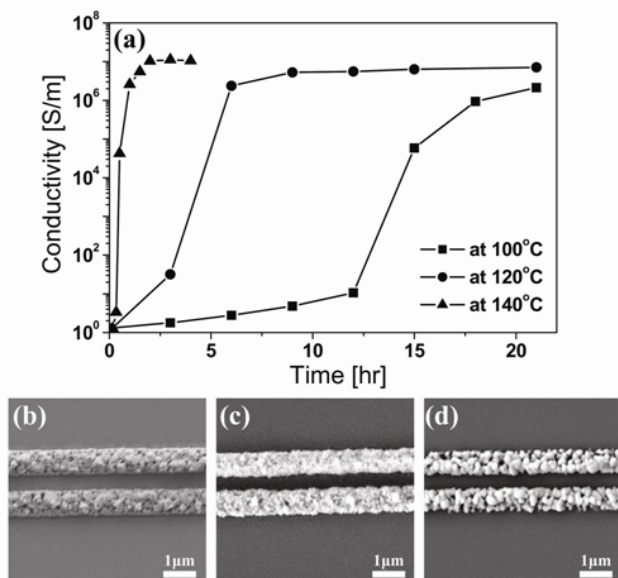


**Figure 3.** (a) The changes in electrical conductivity with time at different annealing temperatures. SEM images of metal nanoparticle patterns after annealing (b) at 100 °C for 20 h, (c) at 120 °C for 8 h and (d) at 140 °C for 2 h.

such as cracks and vacancies along the nanowire originating from the aggregation of the metal nanoparticles within the patterns [15]. Meanwhile, the morphological changes of the silver nanowires were not significant when annealed at 100 and 120 °C. Although annealing at 140 °C was favorable in terms of the fast ramping time to reach the saturated conductivity, it caused a discontinuous current path; this becomes more serious when treating the nanoscale metal nanoparticle patterns. On the other hand, the sample annealed at 100 °C for 20 h could not reach the saturation region of conductivity. Therefore, the optimized annealing condition for Ag NP nanowires was determined to be 120 °C for 8 h, which demands a longer time for sintering compared with other previous reports where much larger and thicker metal nanoparticle patterns (a few tens of micrometers) deposited by ink-jet printing were sintered at harsh temperatures [16]. Because we dealt with thin (250 nm) and narrow (500 nm) metal nanoparticle patterns, extremely mild annealing conditions were used for the metal continuity in spite of the drawback of the extra time required. In addition, metal nanoparticle patterns with an adequate thickness are initially desired in view of volume shrinkage during the annealing. Otherwise, the morphological defects, cracks and vacancies, appeared readily.

In order to confirm the current flow through the metal nanowires annealed at each annealing temperature, we measured the current flow through the 500 nm wide, 250 nm thick nanowires by applying a voltage between the two electric pads using a semiconductor parameter analyzer (Agilent Technologies B1500A). Voltages were applied from  $-0.1$  to  $0.1$  V with a 2 mV step. As expected, the metal nanowire annealed at 140 °C could not carry any electrical current, due to the metallic discontinuities along the nanowire. The current measurements for the metal nanowires annealed

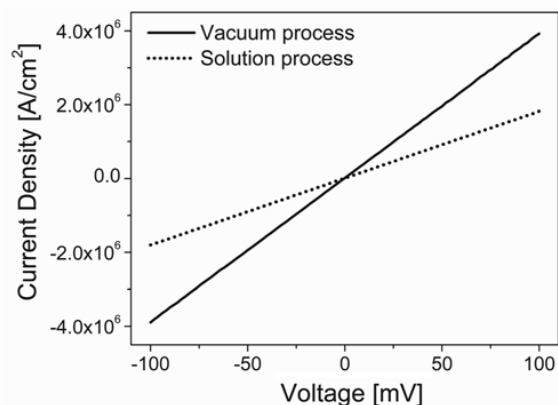


**Figure 4.** Current density–voltage ( $J$ – $V$ ) curves of silver nanowires fabricated by the two methods—the metal nanoparticle solution process and electron-beam evaporation.

at 120 °C suggest that the metal nanoparticles were well-interconnected and formed continuous paths with a current of 1–2 mA at 0.1 V, which is appropriate for electrical applications. For comparison, the same silver patterns (30 nm thickness) were fabricated by electron-beam deposition to the polymer template and a subsequent lift-off process. Current density was directly compared rather than current to eliminate the effect of the difference in nanowire thickness. As shown in figure 4, the current density through the vacuum-processed metal nanowire is twice that through the solution-processed one.

Energy-dispersive x-ray spectroscopy (EDX) analysis was also performed to gain further insight into the effects of annealing on the Ag NP nanowires. We investigated the variation in silver-to-carbon content during the annealing process at 120 °C. The weight percentage of silver to carbon changed from 49.6:50.4 to 84.0:16.0. This indicates that the dispersant was not completely removed during the annealing process, causing a current density lower than that of the vacuum-processed metal nanowire.

The metal electrodes annealed at 120 °C were used as S/D electrodes for P3HT-based OFETs. To compare the properties of the P3HT transistor with the solution-processed S/D electrodes, a reference device with the same configuration was fabricated with electron-beam evaporated silver S/D electrodes. It should be noted here that the other experimental conditions were nearly the same, except for the metal deposition method.

Both P3HT OFETs showed typical p-channel transistor behavior, as shown in figure 5. The device properties, such as the field effect mobility ( $\mu_{\text{FET}}$ ) and threshold voltage ( $V_{\text{th}}$ ), were obtained using the standard formulae for FETs [17]. The P3HT transistors with the solution-processed silver S/D electrodes showed an almost eight-fold increase in the drain current at the same gate and S/D voltages compared to the devices with the evaporated silver electrodes (figures 5(a) and (b)). The calculated  $\mu_{\text{FET}}$  and  $V_{\text{th}}$  values are about  $5.2 \times 10^{-4} \text{ cm}^2 \text{ V}^{-1} \text{ s}^{-1}$ , 12 V and  $6.6 \times 10^{-5} \text{ cm}^2 \text{ V}^{-1} \text{ s}^{-1}$ , 11.6 V for the OFETs with solution-processed and vacuum-deposited

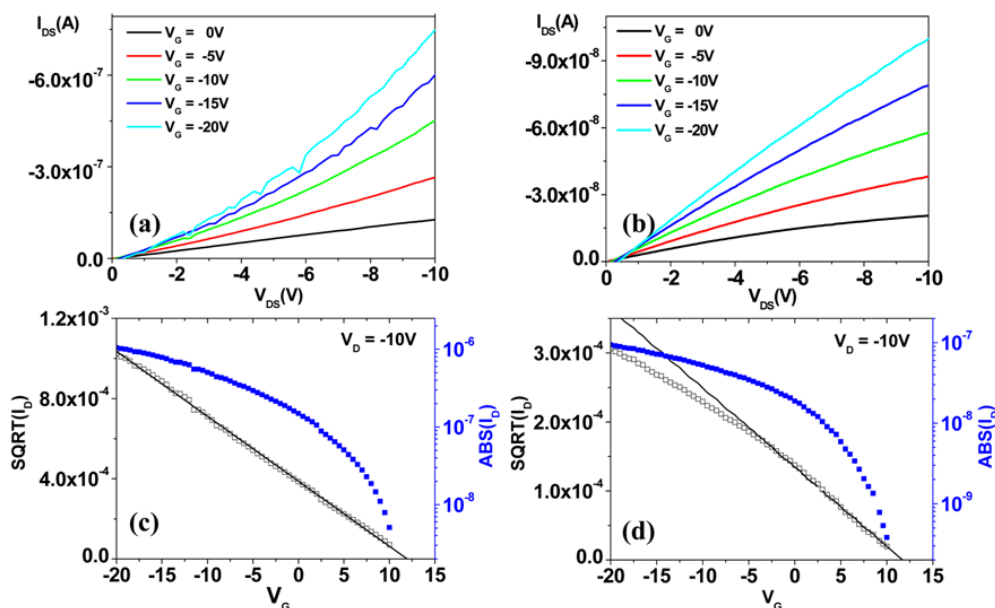


**Figure 5.** Output and transfer characteristics of P3HT OFETs ( $L/W = 300 \text{ nm}/20 \mu\text{m}$ ) with solution-processed ((a) and (c)) and electron-beam evaporated silver S/D ((b) and (d)) electrodes.

silver S/D electrodes, respectively (figures 5(c) and (d)). The mobility is within the expected range and similar to the values reported by other groups for thiophene-based FETs with vacuum-deposited S/D electrodes at a sub-100 nm channel length [18, 19]. The larger drain current and mobility in the P3HT FETs with the solution-processed S/D electrodes could be a result of the thickness difference of the S/D electrodes, providing a different charge injection area.

It should be noted that the relatively low device performances, when compared with the performance of conventional P3HT OFETs with micrometer-sized channel lengths defined by photolithography, were mainly due to a high contact resistance [20, 21]. When the channel length of the transistor is severely reduced, the contact resistance exceeds the channel resistance and becomes a critical factor in the device performance [22]. The sub-linear increase at the low drain voltage ( $V_d$ ) region in the output curve, figure 5(a), indicates that a large contact resistance between the silver S/D electrodes and the P3HT active channel layer limited the efficiency of mobile charge injection. This phenomenon is commonly observed in p-channel OTFTs with low work function metal electrodes, such as silver (work function: 4.5 eV). Moreover, the formation of silver oxide on top of the S/D electrodes during the thermal annealing process could also affect the contact resistance. The super-linear characteristics at the higher  $V_d$  region can be explained by the short-channel (less than  $1 \mu\text{m}$ ) effect. In this study, the high lateral electric field loaded by  $V_d$  due to the short-channel length became comparable to the vertical electric field caused by  $V_g$ , thereby showing the non-saturation behavior in the output curve.

#### 4. Conclusion

An alternative method is proposed in this research for fabricating nanoscale metallic wires using a metal nanoparticle

solution process in combination with a nanoimprint lithography technique. Nanoimprint lithography was chosen due to the ease of preparation of nanoscale polymer templates, where the metal ink was confined and prevented from spreading. The 500 nm wide silver nanoparticle patterns were defined after lift-off and then converted into conducting metallic wires after mild annealing at  $120^\circ\text{C}$ . The developed technique was applied for fabricating the S/D electrodes of P3HT OFETs with a channel length of 300 nm. All fabrication processes avoid the high-vacuum system for metal deposition and are performed at low temperature and pressure, giving a potential continuous process for fabricating low-cost and high-throughput plastic electronics.

#### Acknowledgments

This research was supported by the Korea Research Foundation (KRF-2006-331-D00125) and the Korea Science and Engineering Foundation (KOSEF) NCRG grant funded by the Korean government (MEST) (no. R15-2008-006-03002-0). The SystemIC 2010 project at GIST and the development of next generation RFID technology for item-level applications (2008-F052-01) at ETRI were funded by the Ministry of Knowledge Economy (MKE).

#### References

- [1] Hebner T R, Wu C C, Marcy D, Lu M H and Sturm J C 1998 *Appl. Phys. Lett.* **72** 519
- [2] Siringhaus H, Kawase T and Friend R H 2001 *MRS Bull.* **26** 539
- [3] Bao Z, Feng Y, Dodabalapur A, Raju V R and Lowinger A J 1997 *Chem. Mater.* **9** 1299
- [4] Garnier F, Hajlaoui R, Yasser A and Srivastava P 1994 *Science* **265** 1684

- [5] Rogers J A *et al* 2001 *Proc. Natl Acad. Sci.* **98** 4835
- [6] Calvert P 2001 *Chem. Mater.* **13** 3299
- [7] Chou S Y, Krauss P R and Renstrom P J 1995 *Appl. Phys. Lett.* **67** 3114
- [8] Ruchloeft P *et al* 1999 *J. Vac. Sci. Technol. B* **17** 2965
- [9] International Technology Roadmap for Semiconductors 2003 *Lithography*
- [10] Ko S H, Park I K, Pan H, Grigoropoulos C P, Pisano A P, Luscombe C K and Frechet J M J 2007 *Nano Lett.* **7** 1869
- [11] Park I K, Ko S H, Pan H, Grigoropoulos C P, Pisano A P, Frechet J M J, Lee E S and Jeong J H 2008 *Adv. Mater.* **20** 489
- [12] Jung G Y *et al* 2006 *Nano Lett.* **6** 351
- [13] Jung G Y, Li Z, Wu W, Chen Y, Olynick D L, Wang S Y, Tong W M and Williams R S 2005 *Langmuir* **21** 1158
- [14] Buffat P and Borel J P 1976 *Phys. Rev. A* **13** 2287
- [15] Greer J R and Street R A 2007 *Acta Mater.* **55** 6345
- [16] Perelaer J, de Laat A W M, Hendriks C E and Schubert U S 2008 *J. Mater. Chem.* **18** 3209
- [17] Sze S M 1981 *Physics of Semiconductor Devices* (New York: Wiley)
- [18] Austin M D and Chou S Y 2002 *Appl. Phys. Lett.* **81** 4431
- [19] Collet J, Tharaud O, Chapoton A and Vuillaume D 2000 *Appl. Phys. Lett.* **76** 1941
- [20] Chua L L, Ho P K H, Siringhaus H and Friend R H 2004 *Appl. Phys. Lett.* **84** 3400
- [21] Frank D J, Dennard R H, Nowak E, Solomon P M, Taur Y and Wong H S P 2001 *Proc. IEEE* **89** 259
- [22] Noh Y-Y, Zhao N, Caironi M and Siringhaus H 2007 *Nat. Nanotechnol.* **2** 784